A Gerischer Phase Element in the Impedance Diagram of the Polymer Electrolyte Membrane Fuel Cell Anode†

Anne-Kristine Meland, Dick Bedeaux,* and Signe Kjelstrup

Department of Chemistry, Norwegian University of Science and Technology, 7491 Trondheim, Norway

Received: February 4, 2005; In Final Form: June 21, 2005

We study the isothermal hydrogen adsorption and reaction at the E-TEK electrode of a polymer electrolyte fuel cell with a Nafion 117 membrane by impedance spectroscopy at 30 °C. We find that the impedance diagram must include a Gerischer phase element. Constant phase elements are not sufficient to describe the experimental data. This means that an adsorption reaction takes place in combination with surface diffusion of hydrogen in the carbon layer located before the platinum surface, separate from the charge transfer step at the platinum particle surface. We are not able to distinguish between molecular or atomic hydrogen diffusion on carbon. We predict and find that the relaxation time of the adsorption step is independent of the applied potential. Water may also enter rate-limiting steps in the electrode reaction, but its role needs further clarification.

1. Introduction

Electrochemical impedance spectroscopy (EIS) is an experimental technique that can separate phenomena with different relaxation times, and is thus useful for determination of rate-limiting steps at electrode surfaces.[1] It has been widely used, also in studies of rather complicated three-phase contacts.[2,3] Such contacts are typical for fuel cell electrodes.

Most polymer fuel cell electrodes consist of a porous matrix of carbon black that allow gas diffusion up to the catalyst (Pt) particles. The carbon layer is up to a few hundred micrometers thick.[4] The gas will eventually react at the catalyst, which is also in contact with the proton-conducting membrane electrolyte. This contact is often enhanced by adding a membrane polymer solution to the catalyst layer, as described for instance in the Experimental Section. A complicating factor is the required presence of water in the membrane.[2,5]

Impedance studies on fuel cells have mostly concerned rate-limiting processes in the complete cell.[2,6,7] The cathode, or the oxygen electrode, will then dominate the spectrum. We shall study the anode of the fuel cell, the hydrogen electrode in a cell with two identical hydrogen electrodes. Recent impedance studies of this electrode have been motivated by the need to understand the CO tolerance of this electrode.[8,9] As a background for such studies, it is important to have a good understanding of the elementary steps concerning hydrogen alone. Also, with the present discussion on the mode of hydrogen adsorption in carbon nanotubes,[10] it is interesting to see if impedance studies can provide information about the role of carbon in the anode reaction.

The aim of this investigation is to give experimental and theoretical support to the first step in the anode reaction. We shall see that this must include a reversible reaction (the adsorption reaction) followed by diffusion of the adsorbed species to the site where the charge transfer takes place. The adsorption reaction takes place in a layer with a thickness estimated to be ∼200 μm, located around the Pt particles. Such an adsorption reaction has earlier been allocated to the Pt particle itself; see, for example, the work of Chen and Kucernak,[11] who studied insulated Pt particles.

Various methods have been used to establish a theoretical background for the impedance of a porous electrode. The porous electrode model, e.g., Weber and Newman,[12] consists of a network of normal and charge transfer resistors. Taylor expansions around point values of nonlinear equations for reaction kinetics have long been used to find the impedance.[1,6,13] Gomadam et al.[7] derived impedances for composite electrode models, which treat the composite electrode as a superposition of two continuous phases; one phase is a pure ion conductor, and the other phase is a pure electronic conductor. The fractal structure of these materials can also explain the typically depressed semicircles.[14]

Pugazhendi et al.[3] divided the heterogeneous region into bulk parts and surfaces, and treated the surface as a two-dimensional system according to the method of Gibbs,[15] with surface properties integrated out to give excess variables. The excess energy dissipation at the electrode (or the excess entropy production) of the surface was used in the derivation of the surface impedance. We shall use this method, which is always in agreement with the second law of thermodynamics.

The aim of the study is then, from a chosen model, to first predict an impedance spectrum of the anode. We shall next use the obtained relations to obtain properties of the electrode from experimental results. We shall see that the experiments give support a reaction-diffusion step as the first step in the electrode reaction. We report findings for a common membrane electrode assembly, namely, the E-TEK electrode with 0.5 mg of Pt/cm^2 and a Nafion 117 membrane. It is common to assume that the rate-limiting process in the electrode backing of the anode (as well as the cathode) is diffusion in the gas phase.[2,6,8] The good fit of the data that we obtain to a Gerischer phase element indicates that the reversible adsorption reaction of hydrogen to carbon black along the pore walls and the subsequent diffusion along the surface to the catalyst plays a more important role than has been assumed previously. Gerischer phase elements have been observed for porous electrodes before, but only in

† Part of the special issue "Irwin Oppenheim Festschrift".

* To whom correspondence should be addressed. E-mail: bedeaux@phys.chem.ntnu.no.

10.1021/jp050635q CCC: $30.25
Published on Web 07/30/2005

the solid oxide fuel cell.[16,17] The results do not discriminate between molecular or atomic adsorbed hydrogen.

The paper is organized as follows. We derive the impedance of the hydrogen electrode using a two-layer model in sections 2 and 3. The first layer is that of the porous carbon layer supporting the catalyst particles, the so-called adsorption−diffusion layer. The next layer is the surface layer of the catalyst, where the charge transfer reaction takes place. The experiments and the results, which confirm this model, are described in sections 4 and 5 and discussed in section 6.

2. The Electrode Reactions

Our theoretical model uses the fact that only a small part of the platinum particle has an interface with the gas in the pores so that only a few active sites are accessible directly from the gas. To reach most of the active sites on the Pt surface, the hydrogen molecules must first adsorb to one of the surfaces involved (the gas−carbon, the gas−membrane, or the gas−Pt surface), and then move to the rest of the Pt surface by diffusion along the mentioned surfaces. They arrive at the active sites after passing some three phase contact lines. Hydrogen molecules cannot go directly to the contact line from the gas phase. This would lead to an infinite velocity of the gas close to the contact line, which is impossible. Early adsorption on a surface is therefore crucial for the hydrogen to reach most of the active sites on the Pt surface. As the area of the Pt surface that is accessible to the gas is only a fraction of the porous carbon surface, we have assumed that the absorption and/or desorption on the walls of the pores is the dominant process in our description. As we shall document, this process is (relatively) slow.

In our model, we assume that hydrogen gas is absorbed continuously along the pores in the carbon matrix:

$$\frac{1}{2}\mathrm{H_2(g)} \rightarrow \frac{1}{2}\mathrm{H_2(a)} \qquad \text{(ad-1)}$$

The adsorption reaction is labeled "ad", and a refers to the anode. Hydrogen proceeds to diffuse along the pore surface to the platinum catalyst, located between the porous carbon matrix and the cation exchange membrane. During the diffusion process, some of the hydrogen desorbs to form molecular hydrogen in the gas phase again. This reversibility in the adsorption−desorption reaction is characteristic of a system that leads to a Gerischer impedance. The reaction for chemisorption

$$\frac{1}{2}\mathrm{H_2(g)} \rightarrow \mathrm{H(a)} \qquad \text{(ad-2)}$$

will lead to the same type impedance.

Most reports assume physisorbed gas molecules, so we proceed with model ad-1 and assume that the adsorption has first-order reaction kinetics in both directions:

$$r(x,t) = k^{\mathrm{a}}_{\mathrm{H_2}} c^{\mathrm{g}}_{\mathrm{H_2}} - k^{\mathrm{d}}_{\mathrm{H_2}} c^{\mathrm{a}}_{\mathrm{H_2}}(x,t) \qquad (1)$$

We use a course-grained description in which both concentrations are given in moles per cubic meter. The concentration $c^{\mathrm{g}}_{\mathrm{H_2}}$ is the gas concentration in the pores times the porosity of the carbon layer. The course-grained concentration $c^{\mathrm{a}}_{\mathrm{H_2}}$ is the surface excess concentration in moles per square meter times the surface area of the pores per unit of volume in inverse meters. The constants $k^{\mathrm{a}}_{\mathrm{H_2}}$ and $k^{\mathrm{d}}_{\mathrm{H_2}}$ are rate constants of the reaction. The reaction

$$\frac{1}{2}\mathrm{H_2(a)} \rightarrow \mathrm{H(s)} \qquad \text{(ad-3)}$$

takes place at the metal surface, denoted s, e.g., Chen and Kucernak,[11] if not before, cf., eq ad-2. In the Volmer mechanism, the surface atom in active sites on the surface of the platinum dissociates into protons in the membrane and electrons in the electronically conducting carbon matrix:

$$\mathrm{H(s)} \rightarrow \mathrm{H^+(m)} + \mathrm{e^-(a)} \qquad \text{(ct)}$$

The charge transfer reaction is labeled ct. A recent discussion of the relevant sites on Pt, which are active in the reaction, is given by Chen and Kucernak.[11]

In summary, we have a model where adsorption takes place in a reaction−diffusion layer located before the catalyst surface, while charge transfer takes place at the metal particle surface, i.e., at the catalyst surface. The thickness of the carbon matrix in the experiment is on the order of 0.2 mm, while the thickness of the catalyst layer is on the order of 0.01 mm. In the theory given below, we use a continuous model for the carbon matrix while it is sufficient to use a sharp interface for the catalyst layer; see Kjelstrup et al.[13] for further explanations.

The reaction Gibbs energy of the adsorption reaction is

$$\Delta_r G^{\mathrm{s}}_{\mathrm{ad}}(x,t) = \frac{1}{2}[\mu^{\mathrm{a}}_{\mathrm{H_2}}(x,t) - \mu^{\mathrm{g}}_{\mathrm{H_2}}] \qquad (2)$$

We assume equilibrium in the reaction (ad-3), giving the relation $2\mu^{\mathrm{s}}_{\mathrm{H}} = \mu^{\mathrm{a}}_{\mathrm{H_2}}(x=0)$ between the chemical potential of hydrogen just before the surface and the chemical potential of atoms at the surface. Here $x = 0$ indicates the position of the catalyst surface. The hydrogen gas in the experiment has a constant (independent of position and time) pressure, leading to a constant $\mu^{\mathrm{g}}_{\mathrm{H_2}}$. The bulk anode is located at negative x values and the membrane at positive x values. In our coarse-grained description, transport takes place along a coordinate normal to the surface of the membrane. All variables are then independent of coordinates parallel to the surface.

To describe the electrochemical processes at the surface, we need the change in Gibbs energy at the surface, due to the neutral species:

$$\Delta_n G^{\mathrm{s}}_{\mathrm{ct}}(t) = -\mu^{\mathrm{s}}_{\mathrm{H}}(t) \equiv -\frac{1}{2}\mu^{\mathrm{a}}_{\mathrm{H_2}}(x=0,t) \qquad (3)$$

For the total electrode reaction, we then have

$$\Delta_n G^{\mathrm{s}} = \Delta_r G^{\mathrm{s}}_{\mathrm{ad}}(x=0,t) + \Delta_n G^{\mathrm{s}}_{\mathrm{ct}}(t) = -\frac{1}{2}\mu^{\mathrm{g}}_{\mathrm{H_2}} \qquad (4)$$

We can take the catalyst surface to be electroneutral, by choosing its thickness such that the adsorptions (in moles per square meter) of protons, $\Gamma_{\mathrm{H^+}}$, and of electrons, $\Gamma_{\mathrm{e^-}}$, are equal. Each excess proton near the metal surface therefore forms a dipole with an excess electron in the metal surface. We define the adsorption of the dipoles by

$$\Gamma_{\mathrm{p}}(t) \equiv \Gamma_{\mathrm{H^+}}(t) \qquad (5)$$

The chemical potential of the dipoles formed by adsorbed proton−electron pairs at the catalyst is given by Bedeaux and Kjelstrup:[18]

$$\mu^{\mathrm{s}}_{\mathrm{p}}(t) \equiv \mu^{\mathrm{s}}_{\mathrm{H^+}}(t) + \mu^{\mathrm{s}}_{\mathrm{e^-}}(t) = \mu^{\mathrm{m}}_{\mathrm{H^+}}(x=0,t) + \mu^{\mathrm{a}}_{\mathrm{e^-}}(x=0,t) \qquad (6)$$

A superscript m indicates a property of the membrane. The

chemical potential of the dipoles is

$$\mu_p^s = \mu_p^{s,0} + 2RT \ln(\gamma_p^s \Gamma_p / \Gamma_p^0) \quad (7)$$

where Γ_p^0 is the standard excess concentration of adsorbed dipoles, γ_p^s is the activity coefficient, and $\mu_p^{s,0}$ is the standard chemical potential.

One often refers to the layer in front of the metal surface containing the protons as the double layer and the excess electron density of the metal surface as the charge density of the surface. Our above description clarifies that these two layers in combination are electroneutral and form a dipole layer. The polarization P^s we find (cf. eqs 9 and 11) is nothing else than the polarization due to the double layer, and the c_p^s used in eq 11 is the capacitance of the double layer.

The charge transfer reaction (eq ct) increases the number of adsorbed dipoles, while the electric current j decreases it; therefore

$$\frac{d}{dt}\Gamma_p = r_{ct}^s - \frac{j}{F} \quad (8)$$

where r_{ct}^s refers to the reaction rate and F is Faraday's constant. The surface polarization in the direction normal to the surface is equal to the dipole concentration times Faraday's constant, F, times the average distance, d_s, between the charges

$$P^s = d_s F \Gamma_p \quad (9)$$

With a constant d_s, it follows that the surface polarization and the adsorption of dipoles depend on each other. By eliminating Γ_p from eq 12, we obtain

$$r_{ct}^s = \frac{1}{F}\left(j + \frac{1}{d_s}\frac{d}{dt}P^s\right) \quad (10)$$

The surface polarization divided by the surface thickness gives the surface potential difference times the capacitance of the dipole layer, c_p

$$\frac{P^s}{d_s} = F\Gamma_p = c_p^s \Delta_s \phi \quad (11)$$

It is common to assume that there is equilibrium for water across the pore channel, across the catalyst surface, and into the membrane. We shall also use this assumption in our first calculation.

3. Electrode Impedance

3.1. Variables in the Oscillating Field. Impedances are measured as a function of the frequency ω of the alternating potential, in the presence of a constant applied potential. The cell under investigation is symmetric, so we consider the potential difference between the anode and the center of the membrane:

$$\Delta\phi = \Delta\phi_{dc} + \Delta\phi_{ac} \exp(i\omega t) \quad (12)$$

The potential difference between the center of the membrane and the cathode is the same. We can disregard the contribution to the emf of the two hydrogen electrodes. They are equal and opposite, and in the total cell potential, they cancel each other. Each contribution is then the sum of the potential difference across one surface and half the membrane:

$$\Delta\phi_{dc} = \Delta_s\phi_{dc} + \frac{1}{2}\Delta_m\phi_{dc} \text{ and } \Delta\phi_{ac} = \Delta_s\phi_{ac} + \frac{1}{2}\Delta_m\phi_{ac} \quad (13)$$

The electric current similarly has a dc and an ac contribution

$$j = j_{dc} + j_{ac} \exp(i\omega t) \quad (14)$$

In the membrane, which conducts by protons, one has

$$\Delta_m\phi_{dc} = r_m j_{dc} \text{ and } \Delta_m\phi_{ac} = r_m j_{ac} \quad (15)$$

The corresponding relation for the potential differences across the surface is derived below.

The surface polarization can also be written as the sum of a stationary and an oscillating contribution

$$P^s = P_{dc}^s + P_{ac}^s \exp(i\omega t) \quad (16)$$

For the dc and ac contributions to r_{ct}^s, this gives the following using eq 14

$$r_{ct,dc}^s = \frac{1}{F} j_{dc} \text{ and } r_{ct,ac}^s = \frac{1}{F}\left(j_{ac} + \frac{i\omega P_{ac}^s}{d_s}\right) \quad (17)$$

3.2. Adsorption−Diffusion Layer in Front of the Catalyst. The time dependence of the concentration of hydrogen at position x in the anode is given by

$$\frac{\partial c_{H_2}^a(x,t)}{\partial t} = -\frac{\partial J_{H_2}^a(x,t)}{\partial x} + \frac{1}{2}k_{H_2}^a c_{H_2}^g - \frac{1}{2}k_{H_2}^d c_{H_2}^a(x,t) \quad (18)$$

where

$$J_{H_2}^a(x,t) = -D_{H_2}^a \frac{\partial c_{H_2}^a(x,t)}{\partial x} \quad (19)$$

is the coarse-grained diffusion flux (in moles per square meter per second) of molecular hydrogen along the surface of the pores in the carbon matrix to the catalyst surface at $x = 0$ and $D_{H_2}^a$ is the diffusion constant (in square meters per second). Equilibrium in the adsorption reaction gives, using eq 3, the equilibrium concentration of adsorbed hydrogen

$$c_{H_2,eq}^a = c_{H_2}^g \frac{k_{H_2}^a}{k_{H_2}^d} \quad (20)$$

The rate coefficients may depend on the state of the surface, whether it is polarized, and on the pressure. The constant hydrogen pressure in the pore gives a constant gas concentration, $c_{H_2}^a$, and therefore also a constant value for $c_{H_2,eq}^a$. We use linear kinetics for the adsorption−desorption reaction. As we will discuss in subsection 6.3, the level of adsorption of hydrogen is well below saturation, so linear kinetics is appropriate for this reaction. We introduce the deviation from the equilibrium concentration

$$c_{H_2}^a(x,t) \equiv c_{H_2,eq}^a + \delta c_{H_2}^a(x,t) \quad (21)$$

Equation 18 then becomes for $\delta c_{H_2}^a$

$$\frac{\partial \delta c_{H_2}^a(x,t)}{\partial t} = D_{H_2}^a \frac{\partial^2 \delta c_{H_2}^a(x)}{\partial x^2} - \frac{1}{2}k_{H_2}^d \delta c_{H_2}^a(x,t) \quad (22)$$

For a dc electric current, eq 22 reduces to

$$0 = D^{a}_{H_2}\frac{\partial^2 \delta c^{a}_{H_2,dc}(x)}{\partial x^2} - \frac{1}{2}k^{d}_{H_2}\delta c^{a}_{H_2,dc}(x) \quad (23)$$

The solution is given by

$$\delta c^{a}_{H_2,dc}(x) = -\frac{j_{dc}}{F\sqrt{2D^{a}_{H_2}k^{d}_{H_2}}}\exp\left(x\sqrt{\frac{k^{d}_{H_2}}{2D^{a}_{H_2}}}\right) \quad (24)$$

where we used

$$2J^{a}_{H_2}(x=0) = r^{s}_{ct,dc} = r^{s}_{ad,dc} = j_{dc}/F \quad (25)$$

We see from eq 24 that $\delta c^{a}_{H_2,dc}$ is negative when $j_{dc} > 0$ and positive when $j_{dc} < 0$.

When the thickness d of the carbon layer is smaller than $\sqrt{2D^{a}_{H_2}/k^{d}_{H_2}}$, one should use the fact that the diffusion flux when $x = -d$ is zero. One must then replace $\exp(x\sqrt{k^{d}_{H_2}/2D^{a}_{H_2}})$ with $\cosh[(x + d)\sqrt{k^{d}_{H_2}/2D^{a}_{H_2}}]/\cosh(d\sqrt{k^{d}_{H_2}/2D^{a}_{H_2}})$ in eqs 24 and 28 and make a similar replacement in eqs 31 and 33. This implies that the mass transport at low frequencies will be reduced compared to the expressions given. The further analysis is not affected.

We use

$$\mu^{a}_{H_2}(x,t) = \mu^{a,0}_{H_2} + RT\ln\left[\frac{c^{a}_{H_2}(x,t)}{c^{a,0}_{H_2}}\right] = \mu^{a,0}_{H_2} + RT\ln\left(\frac{c^{a}_{H_2,eq}}{c^{a,0}_{H_2}}\right) + RT\ln\left[\frac{c^{a}_{H_2}(x,t)}{c^{a}_{H_2,eq}}\right]$$

$$= \mu^{a}_{H_2,eq} + RT\ln\left[\frac{c^{a}_{H_2}(x,t)}{c^{a}_{H_2,eq}}\right] \quad (26)$$

for the chemical potential of hydrogen, where $\mu^{a,0}_{H_2}$ and $c^{a,0}_{H_2}$ are standard values. To linear order in δc^{a}_{H} this gives

$$\mu^{a}_{H_2}(x,t) = \mu^{a}_{H_2,eq} + RT\ln\left[1 + \frac{\delta c^{a}_{H_2}(x,t)}{c^{a}_{H_2,eq}}\right] = \mu^{a}_{H_2,eq} + RT\frac{\delta c^{a}_{H_2}(x,t)}{c^{a}_{H_2,eq}} \quad (27)$$

By introducing eq 24, we obtain

$$\mu^{a}_{H_2,dc}(x) = \mu^{a}_{H_2,eq} - \frac{j_{dc}RT}{Fc^{a}_{H_2,eq}\sqrt{2D^{a}_{H_2}k^{d}_{H_2}}}\exp\left(x\sqrt{\frac{k^{d}_{H_2}}{2D^{a}_{H_2}}}\right) \quad (28)$$

The total Gibbs energy change over the whole layer becomes

$$\Delta_r G_{ad,dc} = \mu^{s}_{H,dc} - \frac{1}{2}\mu^{g}_{H_2} = \frac{1}{2}[\mu^{a}_{H_2,dc}(x=0) - \mu^{a}_{H_2,dc}(x=-\infty)] = -\frac{j_{dc}RT}{2Fc^{a}_{H_2,eq}\sqrt{2D^{a}_{H_2}k^{d}_{H_2}}} \quad (29)$$

$\Delta_r G_{ad,dc}$ gives a contribution to the surface potential drop via $\delta\mu^{a}_{H_2,dc}(x=0)$.

The ac contribution to $c^{a}_{H_2}(x,t)$ is also small. Equation 22 together with eq 19 therefore reduces to

$$i\omega\delta c^{a}_{H_2,ac}(x) = D^{a}_{H_2}\frac{\partial^2 \delta c^{a}_{H_2,ac}(x)}{\partial x^2} - \frac{1}{2}k^{d}_{H_2}\delta c^{a}_{H_2,ac}(x) \quad (30)$$

The solution to eq 30 becomes

$$\delta c^{a}_{H_2,ac}(x) = -A\exp\left[x\sqrt{\frac{k^{d}_{H_2}}{2D^{a}_{H_2}}(1 + i\omega\tau_{ad})}\right] \quad (31)$$

where the relaxation time in the adsorption is

$$\tau_{ad} = \frac{2}{k^{d}_{H_2}} = \frac{2c^{a}_{H_2,eq}}{k^{a}_{H_2}c^{g}_{H_2}} \quad (32)$$

We used eq 20 in the last equality. The constant A in eq 31 must be determined from the boundary condition when $x = 0$. The resulting contribution to the chemical potential, cf. eq 27, due to the ac current is

$$\mu^{a}_{H_2,ac}(x) = RT\delta c^{a}_{H_2,ac}(x)/c^{a}_{H_2,eq} = -\frac{ART}{c^{a}_{H_2,eq}}\exp\left[x\sqrt{\frac{k^{d}_{H_2}}{2D^{a}_{H_2}}(1 + i\omega\tau_{ad})}\right] \quad (33)$$

The contribution due to a small dc current has already been given as the second term on the right-hand side of eq 28.

The total amount of adsorbed hydrogen molecules on the pore surface due to the ac current is

$$n^{a}_{H_2,ac} = \int_{-\infty}^{0}\delta c^{a}_{H_2,ac}(x)\,dx = -A\sqrt{\frac{2D^{a}_{H_2}}{k^{d}_{H_2}(1 + i\omega\tau_{ad})}} \quad (34)$$

The ac contribution to the reaction rate for the adsorption reaction is then given by

$$r^{s}_{ad,ac} = -k^{d}_{H_2}\int_{-\infty}^{0}\delta c^{a}_{H_2,ac}(x)\,dx = -k^{d}_{H_2}n^{a}_{H_2,ac} = A\sqrt{\frac{2D^{a}_{H_2}k^{d}_{H_2}}{1 + i\omega\tau_{ad}}} \quad (35)$$

The corresponding reaction rate for the charge transfer reaction is given by

$$r^{s}_{ct,ac} = 2J^{a}_{H_2}(x=0) = A\sqrt{2D^{a}_{H_2}k^{d}_{H_2}(1 + i\omega\tau_{ad})} = (1 + i\omega\tau_{ad})r^{s,a}_{ad,ac} \quad (36)$$

The ac contribution to the reaction Gibbs energy of the adsorption is

$$\Delta_r G_{ad,ac} = \frac{1}{2}[\mu^{a}_{H_2,ac}(x=0) - \mu^{g}_{H_2,ac}] = \frac{1}{2}\mu^{a}_{H_2,ac}(x=0) = -\frac{ART}{2c^{a}_{H_2,eq}} \quad (37)$$

where we used eq 40. By eliminating A in eq 44 using eq 43, we find

$$\Delta_r G_{ad,ac} = -Z_{ad} F^2 r^s_{ct,ac} \tag{38}$$

where

$$Z_{ad} = \frac{RT}{2F^2 c^a_{H_2,eq}\sqrt{2D^a_{H_2} k^d_{H_2}(1 + i\omega\tau_{ad})}} \tag{39}$$

With chemisorption of atomic hydrogen at the surface (reaction ad-2), the corresponding equation becomes

$$Z_{ad-2} = \frac{RT}{F^2 c^a_{H,eq}\sqrt{2D^a_H k^d_H c^a_{H,eq}\,(1 + i\omega\tau_{ad})}} \tag{40}$$

where the diffusion coefficient, the reaction coefficients, and the equilibrium concentration at the surface now refer to atomic hydrogen, cf. eq ad-2. These are impedances of a Gerischer element, and we shall see that experimental results for the hydrogen electrode of the fuel cell fit well to such an element, while a Warburg element or other elements can only be fitted with larger inaccuracies or do not describe the measurements at all. The expressions show that the impedance becomes smaller as the equilibrium adsorption of the hydrogen to the pore surface in the carbon matrix becomes larger. The two impedances differ in their dependence on this concentration.

3.3. Charge Transfer Reaction at the Catalyst Surface. Consider next the catalyst surface, or the interface between the membrane and the adsorption−diffusion layer in the electrode. The excess entropy production rate of this surface, σ^s_{ct}, contains the information about the surface dynamics. For isothermal conditions, the contribution due to the alternating field is[18]

$$T\sigma^s_{ct,ac} = -j_{ac}\Delta_s\phi_{ac} + i\omega P^s_{ct,ac}\left(\frac{D - D^s_{eq}}{\epsilon_0}\right)_{ac} - r^s_{ct,ac}\Delta_n G^s_{ct,ac} \tag{41}$$

The D in this equation is the displacement field, and ϵ_0 is the dielectric constant of vacuum. The equilibrium displacement field is zero for free charges ($D^s_{eq} = 0$). The displacement field is given by $D = -\epsilon_0\Delta_s\phi_{ac}/d_s$. Using eq 17 for the ac contribution, one obtains

$$T\sigma^s_{ct,ac} = -r^s_{ct,ac}(\Delta_n G^s_{ct,ac} + F\Delta_s\phi_{ac}) \tag{42}$$

The theory of nonequilibrium thermodynamics prescribes that the force and the flux are related by

$$\Delta_s\phi_{ac} + \frac{\Delta_n G^s_{ct,ac}}{F} = -\rho^s_{ct} F r^s_{ct,ac} \tag{43}$$

where ρ^s_{ct} is the resistivity of the charge transfer reaction. The electrochemical reaction rate is normally not related to its driving force by a linear relation. In this experiment, the alternating contributions to the forces are small (±5 mV), however, so we can use a linear theory. Also, it is likely that the combination of the two terms on the right-hand side of eq 42 is smaller in absolute value than one of the terms. The adsorption−diffusion layer has an impact on $\Delta_s\phi_{ac}$, through the chemical potential of hydrogen atoms at position $x = 0$. The resistivity is independent of the driving force, but can depend on the temperature and the polarization induced by the dc field.

The dc contribution to the excess entropy production rate is found using the relations $\omega = 0$ and $j_{dc} = Fr^s_{ct,dc}$. This gives

$$T\sigma^s_{ct,dc} = -j_{dc}\left(\Delta_s\phi_{dc} + \frac{\Delta_n G^s_{ct,dc}}{F}\right) \tag{44}$$

For small dc currents, the linear law is thus

$$\Delta_s\phi_{dc} + \frac{\Delta_n G^s_{ct,dc}}{F} = -\rho^s_{ct} F r^s_{ct,dc} = -\rho^s_{ct} j_{dc} \tag{45}$$

which is exactly the same as that for the ac current (eq 43).

3.4. Surface Impedance and Surface Properties. The impedance of the catalyst surface is defined as

$$Z^s \equiv -\frac{\Delta_s\phi_{ac}}{j_{ac}} \tag{46}$$

Adding eqs 38 and 43 gives

$$\Delta_s\phi_{ac} + \frac{\Delta_n G^s_{ac}}{F} = \Delta_s\phi_{ac} = -(\rho^s_{ct} + Z_{ad}) F r^s_{ct,ac} \tag{47}$$

where we used the fact that the chemical potential of the hydrogen gas is constant, cf. eq 4. It furthermore follows from eqs 10 and 11 that

$$Fr^s_{ct,ac} = j_{ac} + i\omega c^s_p \Delta_s\phi_{ac} \tag{48}$$

By combining eqs 46−48, we obtain the impedance of the surface

$$Z^s = \frac{\rho^s_{ct} + Z_{ad}}{1 + i\omega c^s_p(\rho^s_{ct} + Z_{ad})} \tag{49}$$

When $\omega \to \infty$, we see that

$$Z^s_{\omega\to\infty} = 0 \tag{50}$$

In the experiments presented here, we measure the response of two identically made electrodes and a membrane electrolyte. When a dc current is passing the cell, one electrode will be a sink for hydrogen while the other will be a source for hydrogen. The impedances of the two electrodes are the same, however. Both electrodes therefore give the same contribution to the measurement, also when the electrodes are polarized. In terms of the measured impedance, Z^{cell}, and the membrane impedance, Z^{mem}, the impedance of one electrode is then

$$Z^s = \frac{1}{2}(Z^{cell} - Z^{mem}) \tag{51}$$

The membrane impedance is found from eq 49 by taking the limit of Z^{cell} for $\omega \to \infty$. The results that are calculated for Z^s from eq 51 can be fitted to eq 49 using eq 39 for Z_{ad}.

With the heterogeneous catalyst surface, one may expect a nonideal contribution to the impedance. A constant phase element (CPE) shall thus be used, rather than a capacitance in parallel with the resistance. The CPE is defined by its impedance:

$$Z_{CPE} = \frac{1}{T_{ct}(i\omega)^{\alpha_{ct}}} \tag{52}$$

The phase angle of the CPE is constant and independent of the frequency. When $\alpha_{ct} = 1$, $T_{ct} = c^s_p$. The more depressed the

semicircle is, the lower the value of α. We define the relaxation time

$$\tau_{ct} = (T_{ct}\rho_{ct})^{1/\alpha_{ct}} \tag{53}$$

The limiting behavior $\omega \rightarrow 0$ gives

$$Z^{s}_{\omega\rightarrow 0} = Z_{\omega\rightarrow 0,ad} + \rho_{ct} \tag{54}$$

The fit of the experimental results to the theoretical expressions gave Y_0 and τ_{ad} in the following expression for Z_{ad}:

$$Z_{ad} = \frac{1}{Y_0\sqrt{\tau_{ad}^{-1} + i\omega}} \tag{55}$$

where the relaxation time $\tau_{ad} = 2/k^{d}_{H_2}$ (see eq 32). According to eq ad-1, the relaxation time is constant. According to eq ad-2, the corresponding relaxation time depends on the square root of the hydrogen concentration in the gas phase, where $\tau_{ad} = (2k_H c_{H,eq})^{-1} = 2\sqrt{c^{g}_{H_2} k^{a}_{H_2} k_H}$. The admittance is, with adsorption of molecular hydrogen, eq ad-1:

$$Y_0 = \frac{4F^2}{RT} c^{a}_{H_2,eq}\sqrt{D^{a}_{H_2}} \tag{56}$$

and with adsorption of atomic hydrogen, eq ad-2:

$$Y_0 = \frac{F^2}{RT} c^{a}_{H,eq}\sqrt{2D^{a}_{H}\tau_{ad}k^{d}_{H}c^{a}_{H,eq}} = \frac{F^2}{RT} c^{a}_{H,eq}\sqrt{D^{a}_{H}} \tag{57}$$

We see that knowledge of the diffusion constant for the hydrogen molecule (or atom) along the pore enables us to calculate the concentrations of the adsorbed species from the equation given above. The admittance may depend on the applied potential if the kinetic constants and the adsorption depend on this parameter.

4. Experimental Section

4.1. Membrane−Electrode Assembly. The electrodes in this study were both E-TEK gas diffusion electrodes (Elat/Std/DS/V2) with 0.5 mg/cm^2 Pt loading and 20% Pt/C. The electrodes were sprayed with a 5 wt % Nafion solution to give 0.6 mg/cm^2. The cell membrane and electrode assembly (MEA) consisted of two such electrodes separated by a Nafion 117 membrane. The membrane was pretreated using a standard procedure, as described for instance by Møller-Holst.[19] The mechanical pressure over the MEA was 4.2 bar, controlled by a pneumatic cylinder. The same hydrogen pressure of 1 bar was used on the two sides.

The MEA's were tested in a test station developed by Møller-Holst[19] and Vie.[4] The fuel cell was a circular single cell with an active area of 4.91 cm^2. The fuel cell housing was made of stainless steel (SS-316) and was supported by two pistons (SS-316). At the top of the pistons, there were flow fields in a serpentine pattern. The pistons also served as current collectors and thermostats. They contained heating elements. Thermocouples in the cell housing measured the temperature in the electrode backings. The temperatures were controlled by a PID controller (Eurotherm 2408) to 30.0 ± 0.1 °C. The cell voltage was measured between the tops of the pistons.

Care was taken to always use new MEA preparations, as a certain aging effect was observed if the same MEA was used for more than 30 experiments. It has been shown that, for instance, agglomeration of Pt particles takes place over time when the system is under stress,[20] with the important effect that the available surface area is reduced.

4.2. Gas Humidification System. The hydrogen gas (99.999% pure from AGA) was humidified at 80 °C outside the cell, making sure that the gas and MEA were always saturated with water. The gases were humidified in a gas-humidifying system developed by Vie[4] before entering the fuel cell. There are two humidifiers, one for the cathode and one for the anode. The temperatures of the humidifiers were controlled independently of one another.

The dry gas entered at the top of the humidifier tank and was preheated in a heating coil. The gas was then bubbled through a glass sieve and finely dispersed into an 800 mL internal container filled with water at a given temperature. The small internal container was placed in a larger 10 L tank also filled with water. This outer container was heated by an electrical heating tape. This ensures a stable temperature of the gas. The humidified gas left the humidifier at the top of the internal container and entered next the fuel cell system. Saturation of the gases at the given temperature can then be assumed. The humidifying temperature was always higher than the cell temperature to prevent the MEA from drying out when electric current was passing through the cell. A gas flow of 20 mL/min prevented problems with condensing water. This flow rate did not pose any limitations on the observed spectra; see, however, Kim et al.,[9] who studied CO adsorption and found flow rate effects at low gas flow rates.

4.3. Impedance Measurements (EIS). The impedance of the cell described above was measured at 30 °C for five different applied potentials. The applied potentials were 10, 20, 30, 50, and 60 mV. These potentials gave all the small current density required for validity of the theoretical derivations.

The impedance spectra were recorded using a PAR 263A potentiostat and a Solartron 1260 FRA. Z-plot software from Scribner Associates, Inc., was used to run the experiments. Measurements were made in a two-electrode setup. The impedance was obtained by sweeping over the frequency range from 10 kHz to 10 mHz, recording 12 steps/decade for each constant applied potential. An amplitude of 5 mV was used. In our experience, amplitudes larger than this can make a significant change in the spectrum. This is noteworthy, since many investigations are done with an amplitude of ≥10 mV[8]. The current density that corresponded to a particular applied potential was recorded before and after the impedance measurement, to check if the cell was stable. Results were discarded if the current density changed by more than 5%.

4.4. Cyclic Voltammetry (CV). The reproducibility of each cell's performance was also investigated by cyclic voltammetry. Voltammograms were recorded with the PAR 263A and CorrWare software (Scribner) for the same cell as in the impedance experiments. The reference side of the system was then fed with hydrogen gas, while the working side contained nitrogen gas, also 99.999% pure (AGA). Voltammetry experiments were carried out before and after every series of impedance measurements. The scan rate was 50 mV/s, and the applied potential varied between 0.04 and 1.5 V. The temperature was 30 °C. One such voltammogram is shown in Figure 1. It did not change by more than 5% from the start to the end of the series of EIS experiments.

We determined the integral under the curve between the boundary values of 0.4 and 0.05 V, subtracting the constant basis value of 14 mC/cm^2, believed to be due to the electroneutral layer of H(ads).[21] The integration was done with Z-View (Scribner), giving an adsorption of protons of Q_H (mC/cm^2 =

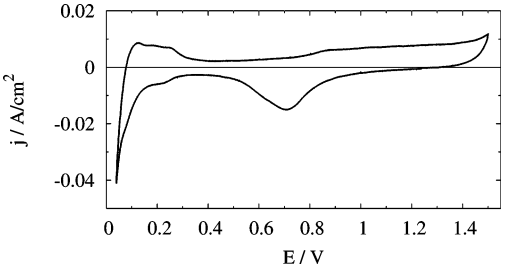

Figure 1. Cyclic voltammetry results for the cell in Figure 2. The working electrode compartment contained pure N_2, and the scan rate was 50 mV/s.

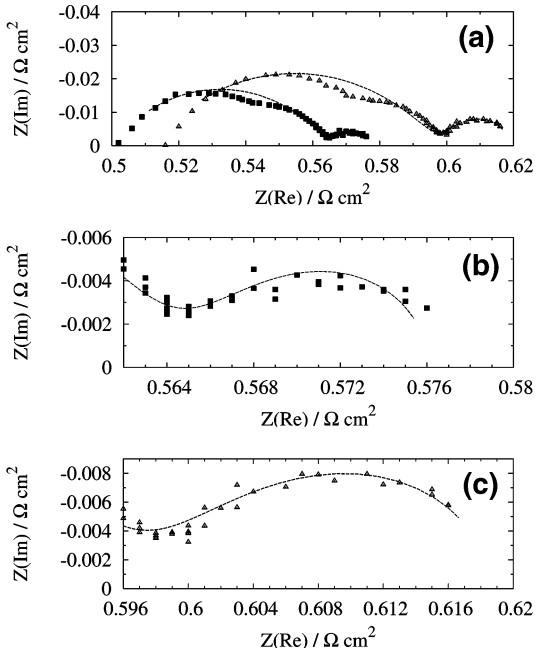

Figure 2. (a) Impedance spectrum of a cell with two identical, new hydrogen fuel cell membrane electrodes and a proton-conducting, water-filled membrane. The electrodes are E-TEK assemblies, and the membrane is Nafion 117. The hydrogen gas saturated with water has a pressure of 1 bar, and the cell temperature is 30 °C. The applied potential is 0 (left curve) and 50 mV (right curve). Lines represent the fitted data. (b) Last arc magnified for the unpolarized electrode. (c) Last arc magnified for the 50 mV experiment.

23 mC/cm^2 or 2.4×10^{-7} mol/cm^2). This charge was converted to a surface area, using as a basis the adsorption of a hydrogen monolayer on bright Pt (210 μC/cm^2 of Pt[21]). For the Pt content used here (0.5 mg of Pt/cm^2), the result was 22 m^2 of Pt/g of Pt. Ciureanu and Wang[8] found an electrochemical surface area of 14 m^2 of Pt/g of Pt in a similar calculation for a surface with a larger Pt loading, while Springer et al.[20] found 24 m^2 of Pt/g of Pt for new MEAs, similar to ours.

These tests all mean that the surface conditions did not change significantly for the series of measurements that were performed. This also means that our MEA can be compared to similar MEAs documented in the literature, and that they therefore appear to be typical for the polymer electrolyte fuel cell anode.

5. Results

The EIS experiments are represented by Figures 2 and 3 and Table 1. The spectra are given as Nyquist plots of Z^{cell} according to

$$Z^{\text{cell}} = Z(Re)^{\text{cell}} + iZ(Im)^{\text{cell}} \tag{58}$$

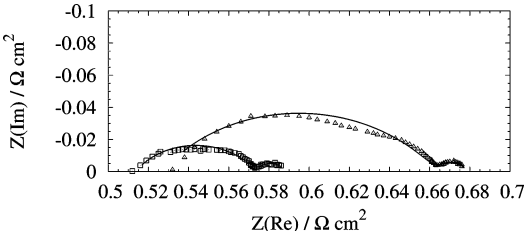

Figure 3. Impedance spectrum of an unpolarized cell with two identical hydrogen fuel cell membrane electrodes and a proton-conducting, water-filled membrane. The electrodes are E-TEK assemblies, and the membrane is Nafion 117. The hydrogen gas saturated with water has a pressure of 1 bar, and the cell temperature is 30 °C. To the left is the impedance of a new MEA, and to the right is the same MEA after 30 experiments. Lines represent the fitted data.

TABLE 1: Fit of Experimental Results for the Fuel Cell Hydrogen Electrode in Figure 2 According to Section 3.4[a]

$\Delta\phi_{dc}$ (mV)	ρ_{ct} (Ω cm^2)	T_{ct} (s$^{\alpha_{ct}}/\Omega^2$)	Y_0 (s$^{1/2}/\Omega$ cm^2)	τ_{ad} (s)
0	0.063 ± 0.002	0.14 ± 0.02	210 ± 30	6
10	0.072 ± 0.003	0.13 ± 0.02	190 ± 20	8
20	0.076 ± 0.003	0.12 ± 0.01	170 ± 20	8
30	0.081 ± 0.003	0.12 ± 0.01	160 ± 20	8
50	0.084 ± 0.003	0.11 ± 0.02	130 ± 10	8
60	0.087 ± 0.004	0.10 ± 0.01	120 ± 10	8

[a] Electrodes are E-TEK, Elat/Std/DS/V2, 0.5 mg of Pt/cm^2, 20 g of Pt/C, impregnated with 0.6 mg of Nafion/cm^2 (5 wt % solution). The membrane is Nafion 117. The cell temperature is 30 °C, and the hydrogen pressure is 1 bar. The applied potential refers to the whole cell. The fits gave all a Nafion membrane area resistance of 0.51 ± 0.01 Ω cm^2, and $\alpha_{ct} = 0.61 \pm 0.02$.

A typical EIS for a cell with unpolarized, new MEAs is shown in Figure 2a (left curve). The spectrum of a cell with an applied dc potential of 50 mV is also shown (right curve). Figure 3 shows the difference between the first and the 30th experiments in an unpolarized cell, i.e., the aging effect of the impedance.

The spectra were fitted as described in section 3.4, and the derived variables are given in Table 1. The variation in the variables of the spectrum with applied potential is seen in detail in this table.

6. Discussion

The first conclusion to be made is that the high-frequency intercept with the real axis in Figure 2 is remarkably constant in all spectra recorded; it is 0.50 ± 0.02 Ω cm^2 in Figure 2a, and does not vary by more than 5% between the samples that have been investigated. The value, which is the resistance of the Nafion 117 membrane in the cell, is in good agreement with results reported in the literature[5] for the same membrane and 25 °C. The reproducible value can be taken as experimental support for a reproducible sample preparation method. We can thus expect the same agglomeration level of catalyst particles, or fractality in the materials, between the samples that were investigated. The absence of inductance is also a good sign. Therefore, despite the complicated heterogeneous structure of the electrode, we believe that the observations reflect real electrochemical processes, rather than instrument artifacts.

6.1. Gerischer Element. Our most interesting experimental finding is the low frequency semicircle in the impedance diagram. We find that this can only be fitted in a meaningful way to a Gerischer phase element. A fit to a Warburg impedance is *not* possible, as such an element does not turn to the axis, but continues at a 45° angle. The behavior seen in Figure 2 is in sharp contrast to results for the hydrogen oxidation reaction on Pt electrodes in acid solutions, a reaction which is diffusion-

controlled.[22] Similarly shaped arcs have been seen before,[9,16] but only Gonzales-Cuenza et al.[16] have used a Gerischer element in their interpretation (for a porous solid oxide fuel cell electrode). A Gerischer element has not previously been reported for this electrode.

Alternative circuits were tried like the Randle's circuit and the same circuit with CPE. When fitted to a Randle's type circuit with two CPE, the last arc gave an α value of 0.50 ± 0.02, a clear indication of a Gerischer type element. None of the alternative fits had the accuracy we found when a Gerischer element was used (around 10% in the fitted variable Y_0; see Table 1). Self-similar (fractal) surfaces have a depressed semicircle; however, it is symmetric unlike the Gerischer.[14,23] In addition, we found studying the aging of the cell that the Gerischer element was unchanged in the experiments (Figure 3). The layer in front of the catalyst is thus not aging, in agreement with the view that aging involves agglomeration of Pt particles.[20] We therefore have confidence in the conclusion that the electrode mechanism must include a step which involves adsorption combined with diffusion. We proceed to discuss possible relevant models in subsection 6.3.

For comparison, Ciureanu and Wang[8] obtained an α value of 0.7 for the second arc in their spectrum. They found that this arc depended neither on the gas flow rates between 20 and 1200 sccm nor on $\omega^{-1/2}$, and allocated the arc to hydrogen adsorption at the Pt surface. In our view, their evidence is not conclusive for such an allocation; see also the discussion below.

In their study of the whole fuel cell, Paganin et al.[2] also found a low-frequency arc at 10 mHz, where we see our second arc. These authors allocated the arc to water diffusion, because it depended on the membrane thickness. This allocation cannot be correct, since such a phenomenon would give a more Warburg-like behavior. Furthermore, the fractal nature of the material can explain a depression like the one described by a constant phase elements, but it cannot explain a Gerischer element.

As a remaining possibility, we discuss the possibility that the present Gerischer element be allocated to reaction and diffusion on the membrane side of the electrode surface. On the membrane side, a reaction must involve charged or polarized species (protons and water). Such processes are not expected to be slow and have a relaxation time on the order of seconds, as observed here.

6.2. High-Frequency Regime. The high-frequency regime of the impedance diagram is, according to the theory of section 3, eq 48, related to the charge transfer step. It is immediately clear, however, that the peak is not a perfect semicircle. In some experiments, it appeared as one depressed semicircle, but in others, like those shown here, a shoulder could be seen on the right-hand side of the (depressed) peak. There is such a shoulder in the unpolarized as well as the polarized electrode (see Figure 2).

The heterogeneity of the electrode may cause a depression of the arc like the one we and others have observed. This has also motivated us and others[8] to fit this part of the circle to a constant phase element. The value of the variable α_{ct} in the fit of the diagram to such an element was 0.61 ± 0.02 for all applied dc potentials (see the heading of Table 1).

The shoulder indicates that a third phenomenon is present. We expect that water may be rate-limiting for the electrode reaction in some contexts. We have assumed that there is equilibrium for water everywhere, but the formation of this equilibrium may not be so fast that this assumption is correct. A rate-limiting role for water, which has been proposed also by others,[2,5,24] requires a revision of the theory given above. We have chosen to postpone a detailed revision of the theory, and focus on the implications of the Gerischer element. For the time being, we regard the first part of the diagram in a qualitative manner. The part reflects the charge transfer step and possibly a proton hydration step. The relaxation times for both possible steps are around a millisecond.

To derive system properties from the diagram, a fit was made as described in section 3.4. Neither T_{ct} nor ρ_{ct} obtained from this fit varied much with the applied potential (see Table 1). The resulting τ_{ct}, calculated using eq 53, is $(4.6 \pm 0.4) \times 10^{-4}$ s for all applied dc potentials. T_{ct} and ρ_{ct} did vary with the number of experiments, however (Figure 3). This may be typical for a low-resistance electrode like the hydrogen electrode. We shall discuss the details in this part of the diagram in a report to come, and return now to the low-frequency part.

6.3. Adsorption Reaction on Pore Walls in the Carbon Backing. A number of questions arise from the conclusion that there is a Gerischer element in the equivalent circuit. If the data show that there is an adsorption−reaction process present, how sure can we be that it takes place along the pore walls in the carbon backing and not at the Pt particles? After all, Chen and Kuzernak[11] found, using Pt on carbon as a catalyst, that an adsorption step took place in front of the charge transfer step on the submicron Pt particles. The carbon was not exposed to hydrogen in this case, however. But, how sure can we be that hydrogen diffuses as a molecule and not as an atom before it reaches the surface? Can we understand the kinetic parameters, which we obtain for the adsorption reaction, for one model but not for the other? And finally, what are the possible consequences of the finding?

Let us discuss the location of the reaction diffusion process first. It is true that equations can be obtained with the exact same form as given above, but with a Gerischer type element valid for the catalyst surface instead as for the porous carbon phase. We need only assume that the reaction (ad) and the diffusion take place at a different location. The consequences of such a shift are several, however, and we shall argue against them below, mainly from implications for the system's properties.

We can first observe that the relaxation time τ_{ad} is constant with the applied dc potential in the experiments (see the last row of Table 1). This is exactly as predicted from eq 32. This fact alone does not favor the carbon backing over the surface as a location for the reaction. We have therefore made the following estimates for the diffusion constant $D^a_{H_2}$ and the variables that follow from knowledge of $D^a_{H_2}$.

With a porosity of the electrode of 0.4,[6] and a pore diameter of 50 nm,[25] the estimated surface area of the pores is 3×10^{-7} m^2 of carbon. The diffusion coefficient of hydrogen in the gas phase is on the order of magnitude of 2×10^{-4} m^2/s.[26] Is this is scaled for the surface volume fraction (taking a surface thickness of 0.33 nm), and a tortuosity of 7,[6] this gives a course-grained value for $D^a_{H_2}$ of 3×10^{-7} m^2/s. We find from Table 1 and eq 56 that the equilibrium concentration of hydrogen at the surface ($c^a_{H_2,eq}$) is 260 mol/m^3 in the unpolarized electrodes, and decreases to 148 mol/m^3 when $\Delta\phi_{dc} = 60$ mV across the cell. The kinetic constant ($k^d_{H_2}$) follows from Table 1 and eq 32 and equals 0.25 s^{-1} for all values of the applied potential. A characteristic length for the reaction−diffusion layer is then

$$l^a_{H_2} = \sqrt{D^a_{H_2}\tau_{ad}} = 1.5 \text{ mm} \qquad (59)$$

Reducing the coarse-grained surface diffusion coefficient by a

factor 10 will increase the concentrations by a factor 3.3 and reduce the characteristic length by the same factor. A monolayer of H_2 corresponds to a coarse-grained concentration of ~3 kmol/m^3. The concentration we calculated above is well below this value, which is reasonable. A characteristic length of 200 μm, comparable to the thickness of the anode backing, would correspond to a diffusion coefficient $D^a_{H_2}$ of 5×10^{-9} m^2/s and be close to a fully occupied monolayer.

The range of probable values can thus explain that reaction, and diffusion takes place across a carbon layer with a thickness characteristic for the fuel cell electrode backing (~200 μm). They are all too large to explain that a similar step takes place at the metal (Pt) particle itself, because these particles are submicron particles.[25] A similar estimate for the Pt surface gives a characteristic length much larger than the size of the particle. We conclude that the Gerischer element cannot be understood by reaction combined with diffusion on the Pt surface. The value obtained by Bae and Lee[27] for the equilibrium adsorption of hydrogen molecules on a carbon molecular sieve ($c^a_{H_2,eq}$) was, for comparison, 4 kmol/m^3 for 1 bar, when adjusting for a density of the carbon sieve of 0.6 g/cm^3.

If the estimates given above hold, the carbon surface plays a more active role in the electrode reaction than hitherto assumed. This may then have a consequence for the design of the electrode. When the access of hydrogen to the three-phase contact line is via the two-phase contact, and this contact can become rate-limiting, the two-phase contact should be made as large as possible.

The results do not give any conclusive information about the state of adsorbed hydrogen on the carbon surface. The mathematical form of the impedance, eq 55, does not distinguish between eqs ad-1 and ad-2. The relaxation time is constant in both models as long as the concentration of hydrogen in the gas in the pores is constant.

Most reports consider physisorption of hydrogen gas on carbonaceous materials. Diffusion of physisorbed molecules may be faster than of chemisorbed atoms, favoring a large value of $l^a_{H_2}$ like we estimate. The value of the admittance Y_0 in Table 1 is sensitive to the applied potential, however. This property depends in the first model (eq ad-1) on the concentration of adsorbed molecules and the surface diffusion constant of H_2. In the second model, the relevant concentration is that of the adsorbed hydrogen atoms. It is likely that the chemisorbed state depends more on the polarization. There is some support for hydrogen adsorption in atomic form on graphite-like forms.[10]

More experiments should be performed to establish relations further. Knowledge about the surface diffusion constant will be helpful. It may be interesting to vary the gas pressure and the temperature. Also important is to study the role of water. Does it play a role in the proton entering the membrane, as indicated by the high-frequency part of the diagram?

7. Conclusion

Electrochemical impedance spectroscopy was performed on the fuel cell electrode E-TEK, Elat/Std/DS/V2, 0.5 mg of Pt/cm^2, 20 g of Pt/C, impregnated with 0.6 mg of Nafion/cm^2 (5 wt % solution). The membrane contact was Nafion 117. The electrode was studied at 30 °C and 1 bar.

We found that a Gerischer element was required to explain the low-frequency part of the electrode impedance. The variables that were deduced from this element support hydrogen adsorption and diffusion along carbon in front of the catalyst where the charge transfer takes place. The data do not allow us to make conclusions about the form of the adsorbed hydrogen. It may be physisorbed or chemisorbed. Experiments that may answer this question were proposed. Water may also enter rate-limiting steps in the electrode reaction, but its role needs further clarification.

Acknowledgment. A.-K.M. is grateful to Nordic Energy Research and Norsk Hydro ASA.

References and Notes

(1) Harrington, D.; Conway, B. *Electrochim. Acta* **1987**, *32*, 1703−1712.
(2) Paganin, V.; Oliveira, C.; Ticianelli, E.; Springer, T.; Gonzalez, E. *Electrochim. Acta* **1998**, *43*, 3761−3766.
(3) Kjelstrup, S.; Pugazhendi, P.; Bedeaux, D. *Z. Phys. Chem.* **2000**, *214*, 895−916.
(4) Vie, P. Characterization and optimization of the polymer electrolyte fuel cell, Thesis, Norwegian University of Science and Technology, Trondheim, Norway, 2002.
(5) Freire, T.; Gonzalez, E. *J. Electroanal. Chem.* **2001**, *503*, 57−68.
(6) Springer, T.; Zawodzinski, T.; Wilson, M.; Gottesfeld, S. *J. Electrochem. Soc.* **1996**, *143*, 587−599.
(7) Gomadam, P.; Weidner, J. W.; Zawodzinski, T. A.; Saab, A. P. *J. Electrochem. Soc.* **2003**, *150*, E371−E376.
(8) Ciureanu, M.; Wang, H. *J. Electrochem. Soc.* **1999**, *146*, 4031−4040.
(9) Kim, J.-D.; Park, Y.-I.; Kobayashi, K.; Nagai, M.; Kunimatsu, M. *Solid State Ionics* **2001**, *140*, 313−325.
(10) Lee, S.; An, K.; Lee, Y.; Seifert, G.; Frauenheim, T. *J. Korean Phys. Soc.* **2001**, *38*, 686−691.
(11) Chen, S.; Kucernak, A. *J. Phys. Chem. B* **2004**, *108*, 13984−13994.
(12) Weber, A.; Newman, J. *Chem. Rev.* **2004**, *104*, 4679−4726.
(13) Kjelstrup, S.; Vie, P.; Bedeaux, D. Irreversible thermodynamics of membrane surface transport with application to polymer fuel cells. In *Surface Chemistry and Electrochemistry of Membranes*; Sørensen, T. S., Ed.; Marcel Dekker: New York, 1999; pp 483−510.
(14) Mulder, W.; Sluyters, J. *Electrochim. Acta* **1988**, *33*, 303−310.
(15) Gibbs, J. *The Scientific Papers of J. W. Gibbs*; Dover: New York, 1961.
(16) Gonzales-Cuenca, M.; Zipprich, W.; Boukamp, B.; Pudmich, G.; Tietz, F. *Fuel Cells* **2001**, *1*, 256−264.
(17) Holtappels, P.; Bradley, J.; Irvine, J.; Kaiser, A.; Mogensen, M. *J. Electrochem. Soc.* **2001**, *148*, A923−A929.
(18) Bedeaux, D.; Kjelstrup, S. *J. Non-Equilib. Thermodyn.* **1999**, *24*, 80−96.
(19) Møller-Holst, S. Solid Polymer Fuel Cells, Thesis, University of Trondheim, Trondheim, Norway, 1996.
(20) Xie, J.; Wood, D., III; Wayne, D.; Zawodzinski, T.; Atanassov, P.; Borpu, R. *J. Electrochem. Soc.* **2005**, *152*, A104−A113.
(21) Biegler, T.; Rand, D.; Woods, R. *J. Electroanal. Chem.* **1971**, *29*, 269−277.
(22) Harrison, J.; Khan, Z. *J. Electroanal. Chem.* **1971**, *30*, 327−330.
(23) le Méhauté, A.; Crepy, G. *Solid State Ionics* **1983**, *9*−*10*, 17−30.
(24) Brown, M.; Primdahl, S.; Mogensen, M. *J. Electrochem. Soc.* **2000**, *147*, 475−485.
(25) Budevski, E. *J. Optoelectron. Adv. Mater.* **2003**, *5*, 1319−1325.
(26) Bird, R.; Stewart, W.; Lightfoot, E. *Transport Phenomena*; Wiley: Chichester, U.K., 1960.
(27) Bae, Y.-S.; Lee, C.-H. *Carbon* **2005**, 95−107.